

One-Nearest Neighborhood Guides Inlier Estimation for Unsupervised Point Cloud Registration

Yongzhe Yuan¹ Yue Wu^{1*} Maoguo Gong² Qiguang Miao¹ A. K. Qin³

¹School of Computer Science and Technology, Xidian University, China

²School of Electronic Engineering, Xidian University, China

³Swinburne University of Technology, Australia

yyz@stu.xidian.edu.cn, {ywu, qgmiao}@xidian.edu.cn, gong@ieee.org, kqin@swin.edu.au

Abstract

The precision of unsupervised point cloud registration methods is typically limited by the lack of reliable inlier estimation and self-supervised signal, especially in partially overlapping scenarios. In this paper, we propose an effective inlier estimation method for unsupervised point cloud registration by capturing geometric structure consistency between the source point cloud and its corresponding reference point cloud copy. Specifically, to obtain a high quality reference point cloud copy, an One-Nearest Neighborhood (1-NN) point cloud is generated by input point cloud. This facilitates matching map construction and allows for integrating dual neighborhood matching scores of 1-NN point cloud and input point cloud to improve matching confidence. Benefiting from the high quality reference copy, we argue that the neighborhood graph formed by inlier and its neighborhood should have consistency between source point cloud and its corresponding reference copy. Based on this observation, we construct transformation-invariant geometric structure representations and capture geometric structure consistency to score the inlier confidence for estimated correspondences between source point cloud and its reference copy. This strategy can simultaneously provide the reliable self-supervised signal for model optimization. Finally, we further calculate transformation estimation by the weighted SVD algorithm with the estimated correspondences and corresponding inlier confidence. We train the proposed model in an unsupervised manner, and extensive experiments on synthetic and real-world datasets illustrate the effectiveness of the proposed method.

1. Introduction

With the rapid development of 3D data acquisition technology, point cloud data collected by LiDAR [42], Struc-

*Corresponding authors.

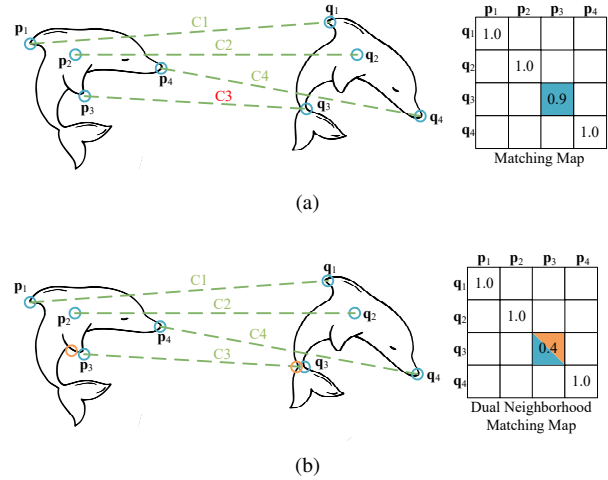


Figure 1. A toy example of **single neighborhood** and proposed **1-NN strategy**. (a) shows that false matching (C3) has very high matching score because of high **single neighborhood** similarity and similar contextual feature. (b) shows that the matching score is adjusted with the help of **1-NN strategy**, and C3 is correctly judged as a false matching.

tured Light Sensors [29], and Stereo Cameras [9] has become ubiquitous in various 3D computer vision and robotics applications [20, 6], such as autopilot [15], surgical navigation [23], and simultaneous localization and mapping [11]. In such applications, rigid body point cloud registration plays an essential role, which aims to find a rigid transformation to align one point cloud to another.

The recent advances have been dominated by learning-based methods. Most of these methods focus on solving the point cloud registration task in a supervised manner [21, 40, 33, 16, 39]. They require labeled data as the supervision signal to learn effective representations. However, obtaining labeled data is cumbersome and time-consuming, which may hinder applications in real scenarios. To address this limitation, unsupervised point cloud registration

methods gradually attract scholars’ attention. Global alignment difference is a widely used optimization signal in unsupervised methods, which learns the optimal rigid transformation to align point cloud pair perfectly by minimizing Chamfer Distance [24, 43]. Nevertheless, Chamfer Distance is very sensitive to the presence of outlier and cannot provide effective self-supervised signal to guide inlier estimation on partially overlapping point cloud.

To tackle issues mentioned above, we propose an effective inlier estimation method for unsupervised point cloud registration by capturing geometric structure consistency between source point cloud and its corresponding reference point cloud copy. Two crucial questions remain to be addressed in order to make unsupervised inlier estimation a success: *How to obtain a high quality corresponding reference point cloud copy? Can single neighborhood strategy provide reliable matching map to generate reference copy?*

We provide answers to both questions. Our key insight is that relying solely on single neighborhood is unreliable to generate matching map. As shown in Figure 1(a), the false matching C3 is mistakenly identified as a correct one due to high single neighborhood similarity and similar contextual feature. Interestingly, introducing the closest point neighborhood of raw point to aid judgement can greatly alleviate this dilemma. The reason is that at least one of raw point and closest point has correct matching. Even if two points are both false matching, integrated dual neighborhood matching score in the matching map is typically quite small and the real impact is limited. We define this strategy as One-Nearest Neighborhood (1-NN) shown in Figure 1(b). The dual neighborhood matching score of C3 has decreased due to low matching score of 1-NN strategy and thus C3 is correctly judged as a false matching.

Motivated by the discussion above, we propose the dual neighborhood fusion matching module to facilitate matching map construction and integrate dual neighborhood matching scores to generate high quality reference point cloud copy. This module employs a 1-NN strategy, which selects the closest point from the input point cloud to generate a 1-NN point cloud. Benefiting from the high quality reference copy, the neighborhood graph formed by inlier and its neighborhood should have consistency between source point cloud and its corresponding reference copy, and outlier is just the opposite. Based on this observation, we propose the geometric neighborhood inlier estimation module to construct effective transformation-invariant geometric structure representations and capture their consistency to score the inlier confidence for each estimated correspondences between source point cloud and its corresponding reference copy. This module provides simultaneously effective byproduct as self-supervised signal based on geometric structure for model optimization. To demonstrate efficacy of the proposed method, we conduct extensive ex-

periments on the synthetic datasets ModelNet40 [35], Augmented ICL-NUIM [7] and real-world dataset 7Scenes [41]. Experimental results illustrate capturing geometric structure consistency between the source point cloud and its corresponding reference copy is effective for inlier estimation. To summarize, our contributions are as follows:

- We propose the dual neighborhood fusion matching module to facilitate matching map construction, which can generate high quality reference copy for source point cloud.
- Based on high quality reference copy, we design a geometric neighborhood inlier estimation module to score the inlier confidence for each estimated correspondences between source point cloud and its reference copy.
- In the unsupervised setting, instead of using the ground-truth transformation, we construct geometric structure consistency objective based on transformation-invariant self-supervised signal for model training and optimization.

2. Related Work

Traditional point cloud registration methods. Most traditional methods need a good initial transformation and converge to the local minima near the initialization point. One of the most profound methods is the Iterative Closest Point (ICP) algorithm [4], which begins with an initial transformation and iteratively alternates between solving two trivial subproblems: finding the closest points as correspondence under current transformation, and computing optimal transformation by SVD [19] based on identified correspondences. Though ICP can complete a high-precision registration, it is susceptible to the initial perturbation. In recent years, variants of ICP have been proposed [30, 38, 5, 14, 27], and they can improve the defects of ICP and enhance the registration accuracy [3]. However, these methods retain a few essential drawbacks. Firstly, they depend strongly on the initialization. Secondly, it is difficult to integrate them into the deep learning pipeline as they lack differentiability. Thirdly, explicit estimation of corresponding points leads to quadratic complexity scaling with the number of points [28], which can introduce significant computational challenges.

Learning-based registration methods. At present, most learning-based methods are based on supervision [33, 40, 26, 12]. PointnetLK [1] is a classical correspondence-free method, which calculates global feature descriptors through PointNet and iteratively uses the Inverse Compositional formulation and LK algorithm (IC-LK) [22, 37] to minimize distance between the descriptors to achieve registration. RPM-Net [39] utilizes the differentiable Sinkhorn

layer and annealing to get soft assignments of point correspondences from hybrid features learned from both spatial coordinates and local geometry.

Recently, unsupervised point cloud registration has gained increasing attention due to its applicability in scenarios where labeled training data is scarce or unavailable. Some methods have been proposed to address this challenge and achieved promising results [18, 10, 8, 2, 17]. Feature-metric point cloud registration framework (FMR) [16] enforces the optimisation of registration by minimizing a feature-metric projection error with a autoencoder-based network. Unfortunately, the registration performance will significantly decline on the partial data due to the lack of inlier estimation. RIE [31] propose a inlier estimation method, which can capture graph-structure difference between source point cloud and the reference point copy generated by single neighborhood strategy for inlier estimation. However, single neighborhood strategy restrains high quality reference point copy generating possibly and thus affect inlier estimation. In comparison, our method achieves stable and reliable reference point copy generating with 1-NN for inlier estimation and can provide effective self-supervised signal for model optimization.

3. Methodology

We first introduce notations utilized throughout this paper. Given two point clouds: source point cloud $\mathcal{P} = \{\mathbf{p}_i \in \mathbb{R}^3 \mid i = 1, \dots, N\}$ and reference point cloud $\mathcal{Q} = \{\mathbf{q}_j \in \mathbb{R}^3 \mid j = 1, \dots, M\}$, where each point is represented as a vector of (x, y, z) coordinates. Point cloud registration task aims to estimate a rigid transformation $\{\mathbf{R}, \mathbf{t}\}$ which accurately aligns \mathcal{P} and \mathcal{Q} , with a 3D rotation $\mathbf{R} \in SO(3)$ and a 3D translation $\mathbf{t} \in \mathbb{R}^3$. The transformation can be solved by:

$$\min_{\mathbf{R}, \mathbf{t}} \sum_{(\mathbf{p}_i^*, \mathbf{q}_j^*) \in \mathcal{H}^*} \|\mathbf{R} \cdot \mathbf{p}_i^* + \mathbf{t} - \mathbf{q}_j^*\|_2^2, \quad (1)$$

where \mathcal{H}^* is the set of ground-truth correspondences between \mathcal{P} and \mathcal{Q} . We propose an effective inlier estimation method for unsupervised point cloud registration by capturing geometric structure consistency between source point cloud and its corresponding reference point cloud copy. To obtain a high quality reference copy, we design dual neighborhood fusion matching module to facilitate matching map construction with 1-NN strategy. Benefiting from the high quality reference copy, we design the geometric neighborhood inlier estimation module to construct effective transformation-invariant geometric structure representations and capture their consistency to score the inlier confidence for each estimated correspondences between source point cloud and its reference copy. The pipeline is illustrated in Figure 2.

3.1. Dual Neighborhood Fusion Matching Module

The matching score is typically calculated by single point feature distance [39] or single neighborhood integration [31] when constructing matching map. These methods may suffer from false matching due to similar contextual feature, as illustrated in Figure 1. In this paper, we propose the 1-NN strategy to generate 1-NN point cloud, which can alleviate this dilemma and facilitate matching map construction for obtaining high quality reference point cloud copy.

We first define 1-NN point cloud $\hat{\mathcal{P}}$ and $\hat{\mathcal{Q}}$ as the closest point for each point in \mathcal{P} and \mathcal{Q} , respectively:

$$\begin{aligned} \hat{\mathcal{P}} &= \{\hat{\mathbf{p}}_i \mid \hat{\mathbf{p}}_i = \arg \min_{\mathbf{p}_m} \|\mathbf{p}_m - \mathbf{p}_i\|_2, i \neq m\}, \\ \hat{\mathcal{Q}} &= \{\hat{\mathbf{q}}_j \mid \hat{\mathbf{q}}_j = \arg \min_{\mathbf{q}_m} \|\mathbf{q}_m - \mathbf{q}_j\|_2, j \neq m\}. \end{aligned} \quad (2)$$

We construct a local patch \mathcal{N}_o with K -nearest neighborhood for each point and extract local features with Dynamic Graph CNN [34] for input point cloud and 1-NN point cloud. Associated learned features are denoted as $\mathcal{F}_{\mathcal{P}}$, $\mathcal{F}_{\hat{\mathcal{P}}}$, $\mathcal{F}_{\mathcal{Q}}$ and $\mathcal{F}_{\hat{\mathcal{Q}}}$, respectively. Then, matching scores are calculated in pairs with the normalized negative feature distance for input point cloud and 1-NN point cloud:

$$\begin{aligned} \mathbf{M}_{i,j} &= \text{softmax}(-\mathbf{D}_{i,1}, -\mathbf{D}_{i,2}, \dots, -\mathbf{D}_{i,M})_j, \\ \widehat{\mathbf{M}}_{i,j} &= \text{softmax}(-\widehat{\mathbf{D}}_{i,1}, -\widehat{\mathbf{D}}_{i,2}, \dots, -\widehat{\mathbf{D}}_{i,M})_j, \end{aligned} \quad (3)$$

where $\mathbf{D}_{i,j} = \|\mathcal{F}_{\mathbf{p}_i} - \mathcal{F}_{\mathbf{q}_j}\|_2$ and $\widehat{\mathbf{D}}_{i,j} = \|\mathcal{F}_{\hat{\mathbf{p}}_i} - \mathcal{F}_{\hat{\mathbf{q}}_j}\|_2$ denote the Euclidean distance between learned local features. Based on the matching scores, we construct dual neighborhood matching map by fusing and averaging matching scores of each \mathcal{N}_o :

$$\mathbf{G}_{i,j} = \frac{1}{K} \sum_{\mathbf{p}_{i'} \in \mathcal{N}_{\mathbf{p}_i}} \sum_{\mathbf{q}_{j'} \in \mathcal{N}_{\mathbf{q}_j}} \mathbf{M}_{i',j'} + \frac{1}{K} \sum_{\hat{\mathbf{p}}_{i'} \in \mathcal{N}_{\hat{\mathbf{p}}_i}} \sum_{\hat{\mathbf{q}}_{j'} \in \mathcal{N}_{\hat{\mathbf{q}}_j}} \widehat{\mathbf{M}}_{i',j'}. \quad (4)$$

A higher matching score indicates consistently larger matching probability, thus highlighting the superior matching quality offered by 1-NN compared to single neighborhood. The explanation is as follows: at least one matching is a correct matching in $\mathbf{M}_{i,j}$ and $\widehat{\mathbf{M}}_{i,j}$, thus leading to a high dual neighborhood matching score in $\mathbf{G}_{i,j}$. Even in cases where $\mathbf{M}_{i,j}$ and $\widehat{\mathbf{M}}_{i,j}$ are all false matching, the dual neighborhood matching score reflected in $\mathbf{G}_{i,j}$ is typically quite small and the real impact is limited. Finally, we formulate the final matching map as:

$$\begin{aligned} \mathbf{F}_{i,j} &= \text{softmax}(-\mathbf{D}'_{i,1}, -\mathbf{D}'_{i,2}, \dots, -\mathbf{D}'_{i,M})_j, \\ \mathbf{D}'_{i,j} &= \exp(\alpha - \mathbf{G}_{i,j}) * (\mathbf{D}_{i,j} + \widehat{\mathbf{D}}_{i,j}), \end{aligned} \quad (5)$$

where $\mathbf{D}'_{i,j}$ is negatively related to the matching score $\mathbf{G}_{i,j}$. We utilize the exponential strategy to control the changing

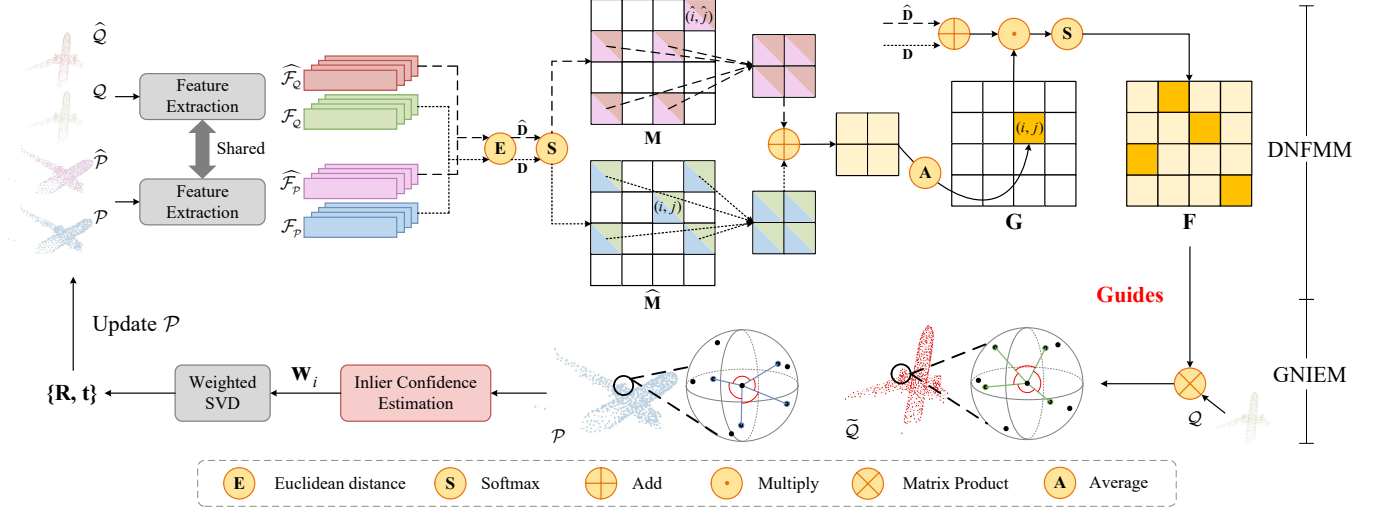


Figure 2. The pipeline of the proposed method. We first extract local features of input point cloud and 1-NN point cloud with DGCNN. The dual neighborhood fusion matching module (DNFMM) aims to facilitate the construction of matching map \mathbf{F} and improve matching confidence for generating high quality reference point cloud copy $\hat{\mathcal{Q}}$. Based on the observation that the neighborhood graph formed by inlier and its neighborhood should have geometric structure consistency between \mathcal{P} and $\hat{\mathcal{Q}}$, the geometric neighborhood inlier estimation module (GNIEM) constructs transformation-invariant geometric structure representations (edge and included angle) and captures their consistency to score the inlier confidence for each estimated correspondences between \mathcal{P} and $\hat{\mathcal{Q}}$. Finally, the transformation is estimated with SVD method via the reliable inliers correspondence.

ratio, along with a hyper-parameter α to control the influence of the dual neighborhood matching [31]. Based on the high quality matching map $\mathbf{F} \in \mathbb{R}^{N \times M}$, we generate a reference point cloud copy $\hat{\mathcal{Q}} \in \mathbb{R}^{N \times 3}$ including matching for each point \mathbf{p}_i in source point cloud \mathcal{P} :

$$\tilde{\mathbf{q}}_i = \sum_{j=1}^M \mathbf{F}_{i,j} \cdot \mathbf{q}_j. \quad (6)$$

Note that Equation 6 means that reference point cloud copy $\hat{\mathcal{Q}}$ contains all predictive correspondences of \mathbf{p}_i in source point cloud. Benefiting from the high quality matching map $\mathbf{F} \in \mathbb{R}^{N \times M}$, reference point cloud copy is also high quality and provides excellent precondition for inlier estimation. In particular, if \mathbf{p}_i is an inlier, the estimated correspondence $\tilde{\mathbf{q}}_i$ will appear in the correct position in reference copy, providing convenience for estimating inlier by capturing geometric structure neighborhood consistency. Conversely, if \mathbf{p}_i is an outlier, the estimated correspondence tends to have an unstable position.

3.2. Geometric Neighborhood Inlier Estimation Module

In this section, we explore the geometric structure neighborhood consistency between the source point cloud and its reference point cloud copy for reliable inlier estimation. As shown in Figure 3, the neighborhood graph formed by inlier and its neighborhood points ($\mathcal{N}_{\mathbf{p}_i}$ and $\mathcal{N}_{\tilde{\mathbf{q}}_i}$) should have consistency between source point cloud and its reference copy.

Conversely, the neighborhood graph formed by outlier has significantly different geometric structure between $\mathcal{N}_{\mathbf{p}_i}$ and $\mathcal{N}_{\tilde{\mathbf{q}}_i}$. Since estimated correspondence $\tilde{\mathbf{q}}_i$ tends to have an unstable position as illustrated in Section 3.1, resulting in a chaotic neighborhood. Based on the above observation, we propose a geometric neighborhood inlier estimation module to construct effective transformation-invariant geometric structure representations, and adaptively capture the geometric structure consistency between $\mathcal{N}_{\mathbf{p}_i}$ and $\mathcal{N}_{\tilde{\mathbf{q}}_i}$ to score the inlier confidence for each estimated correspondences.

We first construct a learnable neighborhood graph by transformation-invariant geometric structure representations of $\mathcal{N}_{\mathbf{p}_i}$ and $\mathcal{N}_{\tilde{\mathbf{q}}_i}$, which consists of edge representation and angle representation:

$$\begin{aligned} \mathbf{e}_{i,k}^{\mathbf{p}} &= \mathbf{p}_i - \mathbf{p}_k, \quad \mathbf{a}_{r,s}^{\mathbf{p}} = \angle(\mathbf{e}_{i,r}^{\mathbf{p}}, \mathbf{e}_{i,s}^{\mathbf{p}}), \\ \mathbf{e}_{i,k}^{\tilde{\mathbf{q}}} &= \tilde{\mathbf{q}}_i - \tilde{\mathbf{q}}_k, \quad \mathbf{a}_{r,s}^{\tilde{\mathbf{q}}} = \angle(\mathbf{e}_{i,r}^{\tilde{\mathbf{q}}}, \mathbf{e}_{i,s}^{\tilde{\mathbf{q}}}), \end{aligned} \quad (7)$$

$i \neq k, k = 1, \dots, K, r, s \in \{1, \dots, K\}$

where \mathbf{p}_k and $\tilde{\mathbf{q}}_k$ are the points in $\mathcal{N}_{\mathbf{p}_i}$, $\mathcal{N}_{\tilde{\mathbf{q}}_i}$. The numerically robust operator $\angle(\cdot_1, \cdot_2)$ computed as:

$$\angle(\cdot_1, \cdot_2) = \text{atan2}(\|\cdot_1 \times \cdot_2\|, (\cdot_1) \cdot (\cdot_2)), \quad (8)$$

which provides results in range $[0, \pi)$. Moreover, these representations express sensitive and discriminative geometric structure in the point cloud, and provide adequate geometric cues for subsequent pipeline.

In order to better capture the neighborhood relevance and promote contextual message propagation, we utilize Multi-

layer Perceptron (MLP) f_θ with parameters θ to fuse representations and characterize the consistency between the neighborhoods by the subtraction of the fused geometric representations:

$$\mathbf{d}_{i,k} = f_\theta \left(\text{concat} \left(\mathbf{e}_{i,k}^{\mathbf{p}}, \mathbf{a}_{r,s}^{\mathbf{p}} \right) \right) - f_\theta \left(\text{concat} \left(\mathbf{e}_{i,k}^{\tilde{\mathbf{q}}}, \mathbf{a}_{r,s}^{\tilde{\mathbf{q}}} \right) \right). \quad (9)$$

Next, we further adaptively learn the attention coefficients $\delta_{i,k}$ of each geometric structure consistency:

$$\delta_{i,k} = \text{softmax} \left(f_\mu \left(\mathbf{d}_{i,1} \right), f_\mu \left(\mathbf{d}_{i,2} \right), \dots, f_\mu \left(\mathbf{d}_{i,K} \right) \right)_k, \quad (10)$$

where f_μ is another MLP with parameters μ . Then, we calculate the inlier confidence \mathbf{w}_i of correspondence $(\mathbf{p}_i, \tilde{\mathbf{q}}_i)$ by aggregating the geometric structure consistency weighted:

$$\mathbf{w}_i = 1 - \text{Tanh} \left(\left| l \left(\sum_{k=1}^K \delta_{i,k} * \mathbf{d}_{i,k} \right) \right| \right), \quad (11)$$

where l is a linear function. Finally, we select the largest N_c weights as reliable inliers correspondence of the source and its reference copy:

$$\mathcal{C}_h = \{ (\mathbf{p}_h, \tilde{\mathbf{q}}_h) \mid h \in \text{topk}(\mathbf{w}_i), i = 1, \dots, N_c \}. \quad (12)$$

We can solve transformation $\{\mathbf{R}_{est}, \mathbf{t}_{est}\}$ in closed form using weighted SVD based on reliable inliers correspondence, which has been shown to be differentiable in [25]:

$$\mathbf{R}_{est}, \mathbf{t}_{est} = \min_{\mathbf{R}, \mathbf{t}} \sum_{(\mathbf{p}_i, \tilde{\mathbf{q}}_i) \in \mathcal{C}_h} \mathbf{w}_i \|\mathbf{R} \cdot \mathbf{p}_i + \mathbf{t} - \tilde{\mathbf{q}}_i\|_2^2. \quad (13)$$

We utilize an iterative scheme to update the source point cloud \mathcal{P} with $\{\mathbf{R}_{est}, \mathbf{t}_{est}\}$.

Besides, this inlier estimation method provides useful byproduct for unsupervised learning, which can be reliable self-supervised signal. More details can be seen in the following section.

3.3. Optimization

We conduct loss function for model optimization, which consists of four part. Then, we train the proposed model in an unsupervised manner instead of using the ground-truth transformations.

Global Consistency Loss. We investigate the global consistency loss between the final transformed source point cloud \mathcal{P}' and the reference point cloud \mathcal{Q} . We utilize the Huber function to assemble the global consistency loss, which is defined as follow:

$$\mathcal{L}_{gc} = \sum_{\mathbf{p}' \in \mathcal{P}'} H_\beta \left(\min_{\mathbf{q} \in \mathcal{Q}} \|\mathbf{p}' - \mathbf{q}\|_2^2 \right) + \sum_{\mathbf{q} \in \mathcal{Q}} H_\beta \left(\min_{\mathbf{p}' \in \mathcal{P}'} \|\mathbf{q} - \mathbf{p}'\|_2^2 \right) \quad (14)$$

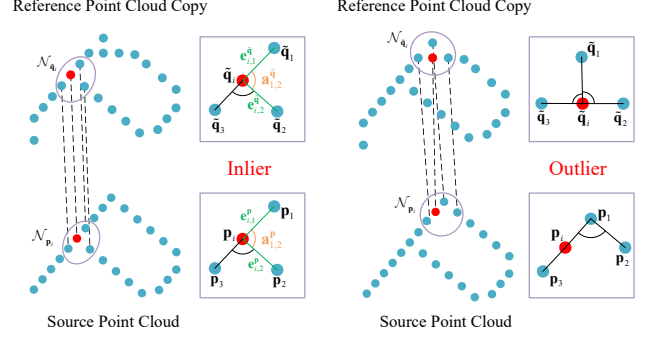


Figure 3. A toy example of inlier and outlier. The neighborhood graph formed by inlier and its neighborhood points should have geometric structure consistency (edge and included angle) between source point cloud and its reference point cloud copy. The outlier is just the opposite.

However, relying solely on global consistency loss is detrimental to the accuracy and reliability of our model. Since the model may still potentially converge to sub-optimization due to the existing outliers, and massive potential information of point cloud is wasted. Hence, it is critical to mine the potential self-supervised signals in the point cloud and construct loss functions based on other existing elements.

Dual Neighborhood Consistency Loss. Based on reliable inliers correspondence in Equation 12, we denote the inliers set of the source and its reference point cloud copy as $\mathbf{X} \in \mathbb{R}^{N_c \times 3}$ and $\mathbf{Y} \in \mathbb{R}^{N_c \times 3}$, respectively. We utilize the neighborhood between the inliers to construct consistency objective, which aims to minimize the registration error between each neighborhood $\mathcal{N}_{\mathbf{x}_i}$ and $\mathcal{N}_{\mathbf{y}_i}$:

$$\mathcal{L}_{in} = \sum_{\mathbf{x}_i \in \mathbf{X}, \mathbf{y}_i \in \mathbf{Y}} \sum_{\mathbf{p}_j \in \mathcal{N}_{\mathbf{x}_i}, \tilde{\mathbf{q}}_j \in \mathcal{N}_{\mathbf{y}_i}} \|\mathbf{R}_{est} \mathbf{p}_j + \mathbf{t}_{est} - \tilde{\mathbf{q}}_j\|_2, \quad (15)$$

where $\mathcal{N}_{\mathbf{x}_i}$ is transformed by $\mathcal{N}_{\mathbf{y}_i}$.

Geometric Structure Consistency Loss. The geometric signal buried in point cloud is readily ignored, which hinders unsupervised inlier estimation. To address this issue, we design a geometric neighborhood loss with the reliable geometric self-supervised signal proposed in Section 3.2:

$$\mathcal{L}_{gs} = \sum_{\mathbf{x}_i \in \mathbf{X}, \mathbf{y}_i \in \mathbf{Y}} \sum_{\mathbf{p}_j \in \mathcal{N}_{\mathbf{x}_i}, \tilde{\mathbf{q}}_j \in \mathcal{N}_{\mathbf{y}_i}} \|\mathbf{e}_{i,j}^{\mathbf{p}} - \mathbf{e}_{i,j}^{\tilde{\mathbf{q}}}\|_2 + \sum_{\mathbf{x}_i \in \mathbf{X}, \mathbf{y}_i \in \mathbf{Y}} \sum_{\mathbf{p}_j \in \mathcal{N}_{\mathbf{x}_i}, \tilde{\mathbf{q}}_j \in \mathcal{N}_{\mathbf{y}_i}} \|\mathbf{a}_{r,s}^{\mathbf{p}} - \mathbf{a}_{r,s}^{\tilde{\mathbf{q}}}\|_2, \quad (16)$$

where $\mathbf{a}_{r,s}^{\mathbf{p}}$ and $\mathbf{a}_{r,s}^{\tilde{\mathbf{q}}}$ is calculated by $\mathbf{e}_{i,j}^{\mathbf{p}}$ and $\mathbf{e}_{i,j}^{\tilde{\mathbf{q}}}$ referring Equation 7.

Spatial Consistency Loss. We further explore to eliminate the spatial difference between the estimated correspondence and the real correspondence for each selected inlier

\mathbf{x}_i and utilize spatial consistency loss with cross-entropy to sharpen matching map:

$$\mathcal{L}_{sc} = -\frac{1}{|\mathbf{X}|} \sum_{\mathbf{x}_i \in \mathbf{X}} \sum_{j=1}^M \mathbb{I}[j = \arg \max_{j'} \mathbf{G}_{i,j'}] \log \mathbf{G}_{i,j}, \quad (17)$$

where $\mathbb{I}[\cdot]$ is the Iverson bracket. Spatial consistency loss encourages to improve the matching probability and thus the estimated correspondence point in reference copy tends to have an stable position.

Since our work utilize an iterative scheme, we compute the loss at each iteration N_l and have the weighted sum loss:

$$\mathcal{L} = \sum_{l=1}^{N_l} (\mathcal{L}_{gc}^l + \gamma \mathcal{L}_{in}^l + \rho \mathcal{L}_{gs}^l + \lambda \mathcal{L}_{sc}^l), \quad (18)$$

where γ , ρ and λ are trade-off parameters to control corresponding loss function.

4. Experiments

4.1. Experimental Setup

We evaluate the proposed method on synthetic datasets ModelNet40 [35] and Augmented ICL-NUIM [7], and real-world dataset 7Scenes [32]. ModelNet40 contains 12,308 CAD models of 40 different object categories. Augmented ICL-NUIM consists of 1,478 synthetic model generated by applying data augmentation on original 739 scan pairs. 7Scenes is a generally used dataset of indoor environment with 7 scenes including Chess, Fires, Heads, Office, Pumpkin, RedKitchen and Stairs.

We compare our method to traditional methods and recent learning-based methods. The traditional methods include ICP [4], FGR [16] and FPFH + RANSAC [13]. The recent learning based methods include IDAM [21], FMR [16], RPMNet [39], CEMNet [17] and RIE [31]. For consistency with previous work, we measure Mean Isotropic Error (MIE) and Mean Absolute Error (MAE). All metrics should be zero if reference point cloud align to source point cloud perfectly.

4.2. ModelNet40 Dataset and Evaluation

We first evaluate registration on ModelNet40, each point cloud contains 2,048 points that randomly sampled from mesh faces and normalized into a unit sphere. We randomly generate three Euler angle rotations within $[0^\circ, 45^\circ]$ and translations within $[-0.5, 0.5]$ on each axis as the rigid transformation during training. Noted that, to simulate partial-to-partial registration, we crop the reference point cloud \mathcal{Q} and the source point cloud \mathcal{P} respectively, and retain 70% of the points. All experiments on ModelNet40 take same settings.

Unseen Objects. Our models are trained and tested on datasets comprising of samples belonging to the same categories, and both the training and test sets are obtained without any preprocessing or manipulation. We apply a random transformation on the reference point cloud \mathcal{Q} to generate corresponding source point cloud \mathcal{P} . Table 1 shows quantitative results of the various algorithms under current experimental settings. The proposed method substantially outperforms all baseline in all metrics. We can observe our method can even outperform the supervised IDAM, RPM-Net and FMR by a large margin. Benefiting from the high quality reference point cloud copy and reliable inlier estimation, our method attains highly accurate registration and improves the registration accuracy by an order of magnitude. In order to show the effect of our proposed approach clearly, a qualitative comparison of the registration results can be found in Figure 4. Our method ensure minimal impact on changing of the shape, and achieve the best performance even on asymmetric shape.

Unseen Categories. To verify the generalization ability on categories, we train the models on the first 20 categories and test on the remaining unseen categories. The results are summarized in Table 1. We can observe that the majority of baseline consistently exhibit lower performance on the unseen categories, especially learning-based methods. In contrast, traditional algorithms are less susceptible to this issue due to the insensitivity of handcrafted methods to shape variance [36]. Our registration process remains highly precise, achieving the lowest error across all metrics, while also maintaining acceptable levels of fluctuation.

Gaussian Noise. In order to assess performance in the presence of noise, which is commonly encountered in real-world point clouds, we train our model on noise-free data and then evaluate all baseline using a test set featuring Gaussian noise. We randomly and independently generate noisy points to introduce noise into in source point cloud and reference point cloud by sampling from $\mathcal{N}(0, 0.5)$ and clipped to $[-1.0, 1.0]$. This experiment is significantly more challenging, as constructing matching map and reference copy become much more difficult. As shown in Table 1, our method outperforms other baseline. In addition, a visualization of registration results can be found in Figure 5. We can observe the Gaussian noise does not affect the registration of main body in point cloud. The experimental results is robust to the noise and indirectly confirms the positive guiding effect of the 1-NN strategy on inlier estimation.

4.3. Other Datasets and Evaluation

We further conduct comparison evaluation on other datasets: 7Scenes and Augmented ICL-NUIM. We sample the reference point clouds to 2,048 points and randomly sample three Euler angle rotations within $[0^\circ, 45^\circ]$ and translations within $[-0.5, 0.5]$ on each axis as the rigid

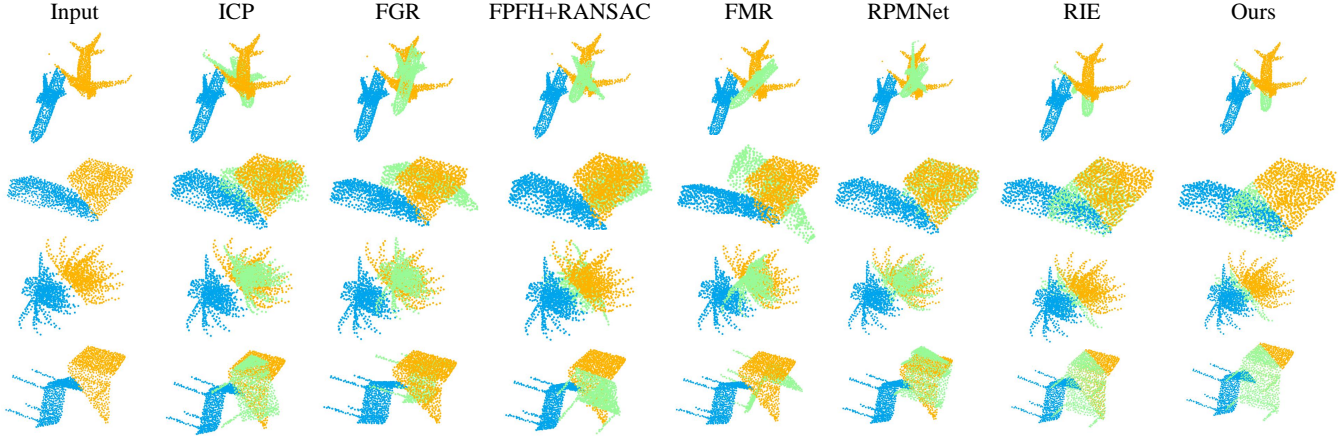


Figure 4. Qualitative comparison of the registration results on unseen objects data (blue: source point cloud, yellow: reference point cloud, green: transformed source point cloud).

Method	Unseen Objects				Unseen Categories				Gaussian Noise			
	MAE(R)	MAE(t)	MIE(R)	MIE(t)	MAE(R)	MAE(t)	MIE(R)	MIE(t)	MAE(R)	MAE(t)	MIE(R)	MIE(t)
ICP [4] (○)	3.4339	0.0114	6.7706	0.0227	3.6099	0.0116	7.0556	0.0228	4.6441	0.0167	9.2194	0.0333
FGR [16] (○)	0.5972	0.0021	1.1563	0.0041	0.4579	0.0016	0.8442	0.0032	1.0676	0.0036	2.0038	0.0072
FPFH+RANSAC [13] (○)	0.7031	0.0025	1.2772	0.0050	0.4427	0.0021	0.9447	0.0043	1.4316	0.0061	2.5345	0.0120
IDAM [21] (▲)	0.4243	0.0020	0.8170	0.0040	0.4809	0.0028	0.9157	0.0055	2.3076	0.0124	4.5332	0.0246
RPMNet [39] (▲)	0.0051	0.0000	<u>0.0201</u>	0.0000	0.0064	0.0001	<u>0.0207</u>	<u>0.0001</u>	0.0075	0.0000	<u>0.0221</u>	<u>0.0001</u>
FMR [16] (▲)	3.6497	0.0101	7.2810	0.0200	3.8594	0.0114	7.6450	0.0225	18.0355	0.0536	35.7986	0.1063
CEMNet[17] (△)	0.1385	<u>0.0001</u>	0.2489	<u>0.0002</u>	0.0804	<u>0.0002</u>	0.1405	0.0003	10.7026	0.0393	21.1836	0.0781
RIE [31] (△)	<u>0.0033</u>	0.0000	0.0210	0.0000	<u>0.0059</u>	0.0000	0.0228	<u>0.0001</u>	<u>0.0069</u>	<u>0.0001</u>	0.0230	<u>0.0001</u>
Ours (△)	0.0006	0.0000	0.0195	0.0000	0.0007	0.0000	0.0182	0.0000	0.0006	0.0000	0.0193	0.0000

Table 1. Evaluation results on ModelNet40. Bold indicates the best performance and underline indicates the second-best performance. (○), (▲) and (△) denote the traditional, supervised and unsupervised methods, respectively.

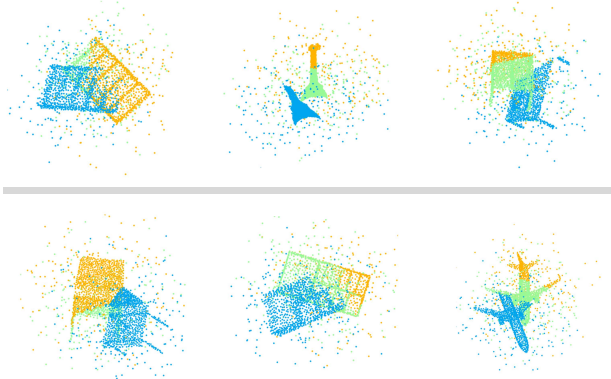


Figure 5. Visualization of registration results on the noisy ModelNet40 (blue: source point cloud, yellow: reference point cloud, green: transformed source point cloud). The gray line is intended to separate the point cloud and prevent scattered points from impacting the clarity of visualization.

transformation to obtain source point clouds, then down-sample the point clouds to 1,536 points to generate the partial data. As demonstrated in Table 3, our method ex-

hibits extremely higher registration precision on all criteria on Augmented ICL-NUIM and 7Scenes, especially the rotation error. Due to space limit, we present more visualization results and quantitative comparison results in appendix. We can summarize our method has best performance and is comfortable with real-world dataset.

4.4. Ablation Study and Analysis

In this section, we conduct extensive ablation studies for a better understanding of the various modules in our method on ModelNet40 and 7Scenes. Due to space limit, we present more ablation studies in appendix.

Dual Neighborhood Fusion Matching Module. We first conduct ablation study on proposed 1-NN point cloud in dual neighborhood fusion matching module. We replace this component with single neighborhood. As shown in the second and seventh rows of Table 2, applying solely the single neighborhood brings no performance gain, since the single neighborhood confuse the matching map and thereby lower the quality of the generated reference point cloud copy. Therefore, we fuse 1-NN point cloud to enhance neighborhood matching map which can promote the gen-

DNFM Module	GNIE Module	\mathcal{L}_{gc}	\mathcal{L}_{in}	\mathcal{L}_{gs}	\mathcal{L}_{sc}	ModelNet40				7Scenes			
						MAE(R)	MAE(t)	MIE(R)	MIE(t)	MAE(R)	MAE(t)	MIE(R)	MIE(t)
✓		✓	✓		✓	0.0919	0.0013	0.1733	0.0026	3.4771	0.0195	7.0834	0.0368
	✓	✓	✓	✓	✓	0.0106	0.0001	0.0271	0.0003	0.0051	0.0000	0.0240	0.0001
✓	✓	✓	✓	✓	✓	0.0020	0.0000	0.0210	0.0000	0.0189	0.0002	0.0282	0.0003
✓	✓	✓		✓	✓	0.1774	0.0018	0.2799	0.0037	0.8186	0.0194	1.5426	0.0375
✓	✓	✓	✓		✓	0.0140	0.0002	0.0343	0.0004	0.0111	0.0001	0.0285	0.0002
✓	✓	✓	✓	✓	✓	0.0103	0.0001	0.0281	0.0002	0.0262	0.0002	0.0455	0.0004
✓	✓	✓	✓	✓	✓	0.0006	0.0000	0.0195	0.0000	0.0036	0.0000	0.0191	0.0001

Table 2. Ablation study of different components on ModelNet40 and 7Scenes. DNFM Module: Dual Neighborhood Fusion Matching Module; GNIE Module: Geometric Neighborhood Inlier Estimation Module; \mathcal{L}_{gc} , \mathcal{L}_{in} , \mathcal{L}_{gs} and \mathcal{L}_{sc} : Each Loss Function in Equation 18.

Method	MAE(R)	MAE(t)	MIE(R)	MIE(t)
Augmented ICL-NUIM				
ICP [4] (○)	2.4022	0.0699	4.4832	0.1410
FGR [16] (○)	2.2477	0.0808	4.1850	0.1573
FPFH+RANSAC [13] (○)	1.2349	0.0429	2.3167	0.0839
IDAM [21] (▲)	4.4153	0.1385	8.6178	0.2756
RPMNet [39] (▲)	0.3267	0.0125	0.6277	0.0246
FMR [16] (▲)	1.1085	0.0398	2.1323	0.0786
CEMNet[17] (△)	0.2374	<u>0.0005</u>	0.3987	<u>0.0010</u>
RIE [31] (△)	<u>0.0492</u>	0.0023	<u>0.0897</u>	0.0049
Ours (△)	0.0005	0.0002	0.0210	0.0004
7Scenes				
ICP [4] (○)	6.0091	0.0130	13.0484	0.0260
FGR [16] (○)	0.0919	0.0004	0.1705	0.0008
FPFH+RANSAC [13] (○)	1.2325	0.0062	2.1875	0.0124
IDAM [21] (▲)	5.6727	0.0303	11.5949	0.0629
RPMNet [39] (▲)	0.3885	0.0021	0.7649	0.0042
FMR [16] (▲)	2.5438	0.0072	4.9089	0.0150
CEMNet[17] (△)	0.0559	<u>0.0001</u>	0.0772	<u>0.0003</u>
RIE [31] (△)	<u>0.0121</u>	<u>0.0001</u>	<u>0.0299</u>	0.0001
Ours (△)	0.0036	0.0000	0.0191	0.0001

Table 3. Evaluation results on Augmented ICL-NUIM and 7Scenes. Bold indicates the best performance and underline indicates the second-best performance. (○), (▲) and (△) denote the traditional, supervised and unsupervised methods, respectively.

eration of correct reference point cloud copy.

Geometric Neighborhood Inlier Estimation Module. We further evaluate the effect of geometric neighborhood inlier estimation module. In this experiment, we do not construct transformation-invariant geometric structure representations for neighborhood but rather utilize raw coordinate to estimation inlier. As shown in the first and seventh rows of Table 2, we can observe coordinate-based method has significantly degraded performance, because coordinate-based method cannot provide transformation-

invariant representations, leading to high stochasticity in inlier estimation. Noted that, geometric neighborhood inlier estimation module provides a self-supervised signal for our model, and \mathcal{L}_{gs} is designed based on this signal. Therefore, when geometric neighborhood is deleted, the loss function \mathcal{L}_{gs} should not participate in optimization.

Loss Function. Comparing 3~6 rows in Table 2, we evaluate the performance of the model with different loss functions. Comprehensively, lacking any part of \mathcal{L} will degrade the performance of the model. The error observed in the fourth row is extremely large, primarily due to the absence of any optimization objective related to transformation in the loss function. This significantly reduces the registration performance of the model. In particular, this ablation study confirms our prediction of \mathcal{L}_{gs} and \mathcal{L}_{sc} can provide reliable and effective self-supervised signal and improve the matching map construction.

5. Conclusion

We propose an effective inlier estimation method for unsupervised point cloud registration, which aims to capture geometric structure consistency between source point cloud and its corresponding reference point cloud copy. We design 1-NN point cloud to potentially facilitate matching map construction for obtaining high quality reference copy. Based on the high quality reference copy, and observation that the neighborhood graph formed by inlier and its neighborhood points should have geometric structure consistency between source and its reference copy, we design a geometric neighborhood inlier estimation module to score the inlier confidence for each estimated correspondence and provide simultaneously the effective self-supervised signal based on geometric structure for model optimization. Finally, we conduct extensive experiments on ModelNet40, Augmented ICL-NUIM and 7Scenes, demonstrating that our unsupervised framework can achieve outstanding performance and 1-NN strategy effectively guides inlier estimation. Moreover, the visualizations of complete predictions demonstrate that the results are faithful and plausible.

References

- [1] Yasuhiro Aoki, Hunter Goforth, Rangaprasad Arun Srivatsan, and Simon Lucey. Pointnetlk: Robust & efficient point cloud registration using pointnet. In *Proceedings of the IEEE/CVF Conference on Computer Vision and Pattern Recognition*, pages 7163–7172, 2019. [2](#)
- [2] Dominik Bauer, Timothy Patten, and Markus Vincze. Reagent: Point cloud registration using imitation and reinforcement learning. In *Proceedings of the IEEE/CVF Conference on Computer Vision and Pattern Recognition*, pages 14586–14594, 2021. [3](#)
- [3] Ben Bellekens, Vincent Spruyt, Rafael Berkvens, Rudi Penne, and Maarten Weyn. A benchmark survey of rigid 3d point cloud registration algorithms. In *Proceedings of International Conference on Ambient Computing, Applications, Services and Technologies*, pages 118–127, 2015. [2](#)
- [4] Paul J Besl and Neil D McKay. Method for registration of 3-d shapes. In *Sensor fusion IV: Control Paradigms and Data Structures*, pages 586–606, 1992. [2](#), [6](#), [7](#), [8](#)
- [5] Sofien Bouaziz, Andrea Tagliasacchi, and Mark Pauly. Sparse iterative closest point. In *Computer Graphics Forum*, pages 113–123, 2013. [2](#)
- [6] Wentao Cheng, Weisi Lin, Xinfeng Zhang, Michael Goesele, and Ming-Ting Sun. A data-driven point cloud simplification framework for city-scale image-based localization. *IEEE Transactions on Image Processing*, 26(1):262–275, 2016. [1](#)
- [7] Sungjoon Choi, Qian-Yi Zhou, and Vladlen Koltun. Robust reconstruction of indoor scenes. In *Proceedings of the IEEE Conference on Computer Vision and Pattern Recognition*, pages 5556–5565, 2015. [2](#), [6](#)
- [8] Mohamed El Banani, Luya Gao, and Justin Johnson. Unsuperviseddr&r: Unsupervised point cloud registration via differentiable rendering. In *Proceedings of the IEEE/CVF Conference on Computer Vision and Pattern Recognition*, pages 7129–7139, 2021. [3](#)
- [9] Jakob Engel, Jörg Stückler, and Daniel Cremers. Large-scale direct slam with stereo cameras. In *IEEE/RSJ International Conference on Intelligent Robots and Systems*, pages 1935–1942, 2015. [1](#)
- [10] Wanquan Feng, Juyong Zhang, Hongrui Cai, Haofei Xu, Junhui Hou, and Hujun Bao. Recurrent multi-view alignment network for unsupervised surface registration. In *Proceedings of the IEEE/CVF Conference on Computer Vision and Pattern Recognition*, pages 10297–10307, 2021. [3](#)
- [11] Nicola Fioraio and Kurt Konolige. Realtime visual and point cloud slam. In *Proceedings of the RGB-D Workshop on Advanced Reasoning with Depth Cameras at Robotics: Science and Systems Conf.(RSS)*, 2011. [1](#)
- [12] Kai Fischer, Martin Simon, Florian Olsner, Stefan Milz, Horst-Michael Gross, and Patrick Mader. Stickypillars: Robust and efficient feature matching on point clouds using graph neural networks. In *Proceedings of the IEEE/CVF Conference on Computer Vision and Pattern Recognition*, pages 313–323, 2021. [2](#)
- [13] Martin A Fischler and Robert C Bolles. Random sample consensus: a paradigm for model fitting with applications to image analysis and automated cartography. *Communications of the ACM*, 24(6):381–395, 1981. [6](#), [7](#), [8](#)
- [14] Andrew W Fitzgibbon. Robust registration of 2d and 3d point sets. *Image and Vision Computing*, 21(13-14):1145–1153, 2003. [2](#)
- [15] Andreas Geiger, Philip Lenz, and Raquel Urtasun. Are we ready for autonomous driving? the kitti vision benchmark suite. In *Proceedings of the IEEE/CVF Conference on Computer Vision and Pattern Recognition*, pages 3354–3361, 2012. [1](#)
- [16] Xiaoshui Huang, Guofeng Mei, and Jian Zhang. Feature-metric registration: A fast semi-supervised approach for robust point cloud registration without correspondences. In *Proceedings of the IEEE/CVF Conference on Computer Vision and Pattern Recognition*, pages 11366–11374, 2020. [1](#), [3](#), [6](#), [7](#), [8](#)
- [17] Haobo Jiang, Yaqi Shen, Jin Xie, Jun Li, Jianjun Qian, and Jian Yang. Sampling network guided cross-entropy method for unsupervised point cloud registration. In *Proceedings of the IEEE/CVF International Conference on Computer Vision*, pages 6128–6137, 2021. [3](#), [6](#), [7](#), [8](#)
- [18] Pranav Kadam, Min Zhang, Shan Liu, and C-C Jay Kuo. Unsupervised point cloud registration via salient points analysis (spa). In *2020 IEEE International Conference on Visual Communications and Image Processing (VCIP)*, pages 5–8, 2020. [3](#)
- [19] Akiyoshi Kurobe, Yusuke Sekikawa, Kohta Ishikawa, and Hideo Saito. Corsnet: 3d point cloud registration by deep neural network. *IEEE Robotics and Automation Letters*, 5(3):3960–3966, 2020. [2](#)
- [20] Huan Lei, Guang Jiang, and Long Quan. Fast descriptors and correspondence propagation for robust global point cloud registration. *IEEE Transactions on Image Processing*, 26(8):3614–3623, 2017. [1](#)
- [21] Jiahao Li, Changhao Zhang, Ziyao Xu, Hangning Zhou, and Chi Zhang. Iterative distance-aware similarity matrix convolution with mutual-supervised point elimination for efficient point cloud registration. In *European Conference on Computer Vision*, pages 378–394. Springer, 2020. [1](#), [6](#), [7](#), [8](#)
- [22] Simon Lucey, Rajitha Navarathna, Ahmed Bilal Ashraf, and Sridha Sridharan. Fourier lucas-kanade algorithm. *IEEE Transactions on Pattern Analysis and Machine Intelligence*, 35(6):1383–1396, 2012. [2](#)
- [23] Longfei Ma, Hanying Liang, Boxuan Han, Shizhong Yang, Xinran Zhang, and Hongen Liao. Augmented reality navigation with ultrasound-assisted point cloud registration for percutaneous ablation of liver tumors. *International Journal of Computer Assisted Radiology and Surgery*, pages 1–10, 2022. [1](#)
- [24] Marlon Marcon, Riccardo Spezialetti, Samuele Salti, Luciano Silva, and Luigi Di Stefano. Unsupervised learning of local equivariant descriptors for point clouds. *IEEE Transactions on Pattern Analysis and Machine Intelligence*, 44(12):9687–9702, 2021. [2](#)
- [25] Théodore Papadopoulos and Manolis IA Lourakis. Estimating the jacobian of the singular value decomposition: Theory and applications. In *European Conference on Computer Vision*, pages 554–570, 2000. [5](#)

- [26] Zheng Qin, Hao Yu, Changjian Wang, Yulan Guo, Yuxing Peng, and Kai Xu. Geometric transformer for fast and robust point cloud registration. In *Proceedings of the IEEE/CVF Conference on Computer Vision and Pattern Recognition*, pages 11143–11152, 2022. 2
- [27] Szymon Rusinkiewicz. A symmetric objective function for icp. *ACM Transactions on Graphics*, 38(4):1–7, 2019. 2
- [28] Szymon Rusinkiewicz and Marc Levoy. Efficient variants of the icp algorithm. In *Proceedings of International Conference on 3-D Digital Imaging and Modeling*, pages 145–152, 2001. 2
- [29] Joaquim Salvi, Jordi Pages, and Joan Batlle. Pattern codification strategies in structured light systems. *Pattern recognition*, 37(4):827–849, 2004. 1
- [30] Aleksandr Segal, Dirk Haehnel, and Sebastian Thrun. Generalized-icp. In *Robotics: Science and Systems*, 2009. 2
- [31] Yaqi Shen, Le Hui, Haobo Jiang, Jin Xie, and Jian Yang. Reliable inlier evaluation for unsupervised point cloud registration. In *Proceedings of the AAAI Conference on Artificial Intelligence*, volume 36, pages 2198–2206, 2022. 3, 4, 6, 7, 8
- [32] Jamie Shotton, Ben Glocker, Christopher Zach, Shahram Izadi, Antonio Criminisi, and Andrew Fitzgibbon. Scene coordinate regression forests for camera relocalization in rgb-d images. In *Proceedings of the IEEE conference on computer vision and pattern recognition*, pages 2930–2937, 2013. 6
- [33] Yue Wang and Justin M Solomon. Deep closest point: Learning representations for point cloud registration. In *Proceedings of the IEEE/CVF International Conference on Computer Vision*, pages 3523–3532, 2019. 1, 2
- [34] Yue Wang, Yongbin Sun, Ziwei Liu, Sanjay E Sarma, Michael M Bronstein, and Justin M Solomon. Dynamic graph cnn for learning on point clouds. *ACM Transactions On Graphics*, 38(5):1–12, 2019. 3
- [35] Zhirong Wu, Shuran Song, Aditya Khosla, Fisher Yu, Linguang Zhang, Xiaoou Tang, and Jianxiong Xiao. 3d shapenets: A deep representation for volumetric shapes. In *Proceedings of the IEEE/CVF Conference on Computer Vision and Pattern Recognition*, pages 1912–1920, 2015. 2, 6
- [36] Hao Xu, Nianjin Ye, Shuaicheng Liu, Guanghui Liu, and Bing Zeng. Finet: Dual branches feature interaction for partial-to-partial point cloud registration. *arXiv preprint arXiv:2106.03479*, 2021. 6
- [37] Heng Yang, Jingnan Shi, and Luca Carlone. Teaser: Fast and certifiable point cloud registration. *IEEE Transactions on Robotics*, 37(2):314–333, 2021. 2
- [38] Jiaolong Yang, Hongdong Li, Dylan Campbell, and Yunde Jia. Go-icp: A globally optimal solution to 3d icp point-set registration. *IEEE Transactions on Pattern Analysis and Machine Intelligence*, 38(11):2241–2254, 2015. 2
- [39] Zi Jian Yew and Gim Hee Lee. Rpm-net: Robust point matching using learned features. In *Proceedings of the IEEE/CVF Conference on Computer Vision and Pattern Recognition*, pages 11824–11833, 2020. 1, 2, 3, 6, 7, 8
- [40] Wentao Yuan, Benjamin Eckart, Kihwan Kim, Varun Jampani, Dieter Fox, and Jan Kautz. Deepgmr: Learning latent gaussian mixture models for registration. In *European Conference on Computer Vision*, pages 733–750, 2020. 1, 2
- [41] Andy Zeng, Shuran Song, Matthias Nießner, Matthew Fisher, Jianxiong Xiao, and Thomas Funkhouser. 3dmatch: Learning local geometric descriptors from rgb-d reconstructions. In *Proceedings of the IEEE/CVF Conference on Computer Vision and Pattern Recognition*, pages 1802–1811, 2017. 2
- [42] Ji Zhang and Sanjiv Singh. Loam: Lidar odometry and mapping in real-time. In *Robotics: Science and Systems*, 2014. 1
- [43] Yiqiang Zhao, Yiyao Zhou, Rui Chen, Bin Hu, and Xiding Ai. Mm-flow: Multi-modal flow network for point cloud completion. In *Proceedings of the 29th ACM International Conference on Multimedia*, pages 3266–3274, 2021. 2